



Longitudinal hotspots in the mesospheric OH variations due to energetic electron precipitation

M. E. Andersson¹, P. T. Verronen¹, C. J. Rodger², M. A. Clilverd³, and S. Wang⁴

¹Earth Observation, Finnish Meteorological Institute, Helsinki, Finland

²Department of Physics, University of Otago, Dunedin, New Zealand

³British Antarctic Survey (NERC), Cambridge, UK

⁴Jet Propulsion Laboratory, California Institute of Technology, California, USA

Correspondence to: M. E. Andersson (monika.andersson@fmi.fi)

Received: 13 June 2013 – Published in Atmos. Chem. Phys. Discuss.: 26 July 2013

Revised: 5 December 2013 – Accepted: 20 December 2013 – Published: 29 January 2014

Abstract. Using Microwave Limb Sounder (MLS/Aura) and Medium Energy Proton and Electron Detector (MEPED/POES) observations between 2005–2009, we study the longitudinal response of nighttime mesospheric OH to radiation belt electron precipitation. Our analysis concentrates on geomagnetic latitudes from 55–72° N/S and altitudes between 70 and 78 km. The aim of this study is to better assess the spatial distribution of electron forcing, which is important for more accurate modelling of its atmospheric and climate effects. In the Southern Hemisphere, OH data show a hotspot, i.e. area of higher values, at longitudes between 150° W–30° E, i.e. poleward of the Southern Atlantic Magnetic Anomaly (SAMA) region. In the Northern Hemisphere, energetic electron precipitation-induced OH variations are more equally distributed with longitude. This longitudinal behaviour of OH can also be identified using Empirical Orthogonal Function analysis, and is found to be similar to that of MEPED-measured electron fluxes. The main difference is in the SAMA region, where MEPED appears to measure very large electron fluxes while MLS observations show no enhancement of OH. This indicates that in the SAMA region the MEPED observations are not related to precipitating electrons, at least not at energies >100 keV, but rather to instrument contamination. Analysis of selected OH data sets for periods of different geomagnetic activity levels shows that the longitudinal OH hotspot south of the SAMA (the Antarctic Peninsula region) is partly caused by strong, regional electron forcing, although atmospheric conditions also seem to play a role. Also, a weak signature of this OH hotspot is seen during periods

of generally low geomagnetic activity, which suggests that there is a steady drizzle of high-energy electrons affecting the atmosphere, due to the Earth's magnetic field being weaker in this region.

1 Introduction

An important source of variability of mesospheric OH at high latitudes comes from energetic particle precipitation events that originate from explosions on the surface of the Sun (Thorne, 1977; Heaps, 1978; Verronen et al., 2006, 2007; Damiani et al., 2008, 2010b; Jackman et al., 2011; Verronen et al., 2011). In contrast to solar protons, which propagate directly from the Sun into Earth's atmosphere, energetic electrons are first stored and energised in the radiation belts. During geomagnetic storms, strong acceleration and loss processes occur (Reeves et al., 2003), which can both boost the trapped population and lead to significant loss of electrons into the atmosphere. Energetic electron precipitation (EEP) from the radiation belts affects the neutral atmosphere at magnetic latitudes of about 55–72° and results in the enhancement of HO_x through water cluster ion chemistry. This process is only effective below about 80 km, where enough water vapour is available (Solomon et al., 1981; Sinnhuber et al., 2012; Verronen and Lehmann, 2013). The atmospheric penetration depth depends on the energy of the particles, e.g. electrons with 100 keV and 3 MeV energy can reach 80 km and 50 km, respectively (see, e.g. Turunen et al., 2009, Fig. 3).

The primary driver of the radiation belt variability is geomagnetic activity, which can come either from the coronal mass ejections (CMEs) during solar maximum or the high-speed solar wind streams (HSSWS, > 500 km/s) which are most common during the declining and minimum phase of solar activity. The energy input to the magnetosphere during HSSWS events is comparable to or can be higher than the energy input during CMEs (Richardson et al., 2000, 2001). Such storms tend to be weaker than CME storms in terms of geomagnetic index values, last longer, and involve more radiation belt dynamics in the production of electron precipitation (Borovsky et al., 2006).

EEP can occur on different timescales with varying significance for the atmospheric chemistry, but our understanding of the nature of the precipitation as well as the variation of the electron flux lost to the atmosphere is limited. This is mostly due to spatial and temporal limitation of the measurements as well as contamination issues in the space-based instrumentation (Rodger et al., 2010a; Clilverd et al., 2010). Therefore, detailed study of the EEP effects in the atmosphere can significantly improve our understanding of the EEP variability which is important for atmospheric modelling (Funke et al., 2011).

Recent studies provided evidence of the connection between precipitating radiation belt electrons and mesospheric hydroxyl (Andersson et al., 2012; Verronen et al., 2011). By analysing zonal mean time series of MLS/Aura OH mixing ratios and MEPED/POES radiation belt electron fluxes during the period August 2004–December 2009, they demonstrated strong correlation between experimentally observed 100–300 keV electron count rates and nighttime OH concentrations below 80 km. These studies provided a lower-limit estimation of the importance of energetic electron precipitation on HO_x , showing that for the considered time period, EEP has measurable effects in about 30 % of cases.

In this paper, we combine MLS OH and MEPED EEP satellite measurements to study the longitudinal OH variations caused by precipitating radiation belt electrons between January 2005–December 2009. We go on to utilise empirical orthogonal function (EOF) analysis to identify OH spatial and temporal patterns of variability. Finally we provide clear evidence that the SAMA region influences the longitudinal variation of OH at geomagnetic latitudes 55 – 72° in the Southern Hemisphere (SH), as expected from the location of the radiation belts and the weaker magnetic field region. Note that the time period 2005–2009 analysed here coincided with declining phase of solar activity and an extended solar minimum, and thus consists mainly of HSSWS-driven storms.

2 Data

2.1 MLS/Aura observations

The MLS instrument onboard NASA's Aura satellite, placed into a Sun-synchronous orbit (about 705 km), samples the atmosphere up to 82° N/S (Waters et al., 2006). MLS observes thermal microwave emission, scanning from the ground to 90 km every 25 s with daily global coverage of about 14.6 orbits per day.

In this study, we use Version 3.3 Level 2 nighttime (solar zenith angle $> 100^\circ$) OH for the time period of January 2005–December 2009 between 70 and 78 km altitude (corresponding to pressure levels between 0.046 and 0.015 hPa). The altitude selection was based on previous studies, i.e. (Andersson et al., 2012), which showed that between 70 and 78 km the response of OH to electron precipitation is the highest. The vertical resolution of OH observations is about 2.5 km and the systematic error is typically less than 10 %. The data were screened according to the MLS data description and quality document (Livesey et al., 2011). The OH observations taken during solar proton events (SPE), which dominate the ionization in the middle atmosphere, were excluded here and from all further considerations using a flux limit of $4 \text{ protons cm}^{-2} \text{ s}^{-1} \text{ sr}^{-1}$ as observed by GOES-11 at 5–10 MeV energies.

In addition, to support our discussion about OH variations, we also use MLS water vapour (H_2O) and temperature observations. The H_2O and temperature data were sampled the same way as the OH measurements and screened according to the MLS data quality document. The vertical resolution of H_2O /temperature observations is coarser than that of OH at considered altitudes, i.e. about 5 km, and therefore, we use measurements between 70 and 76 km (corresponding to pressure levels between 0.046 and 0.025 hPa). The systematic error of the H_2O /temperature data is typically less than about 0.8 ppmv (25 %)/3 K (5 %). Details on the validation of the MLS OH, H_2O and temperature are given in Pickett et al. (2008), Lambert et al. (2007) and Schwartz et al. (2008), respectively. Note that due to the selection criteria we have more observations during the wintertime.

3 MEPED/POES observation

The Space Environment Monitor (SEM-2) instrument package onboard the Sun-synchronous (800–850 km) NOAA POES satellites, provides long-term global measurement of precipitating electron fluxes with some limited energy spectra information. SEM-2 includes the Medium Energy Proton and Electron Detector (MEPED) which consists of two electron telescopes and two proton telescopes. The pairs of telescopes are pointed approximately perpendicular to each other. Both electron telescopes provide three channels of energetic electron data: > 30 keV, > 100 keV, and > 300 keV,

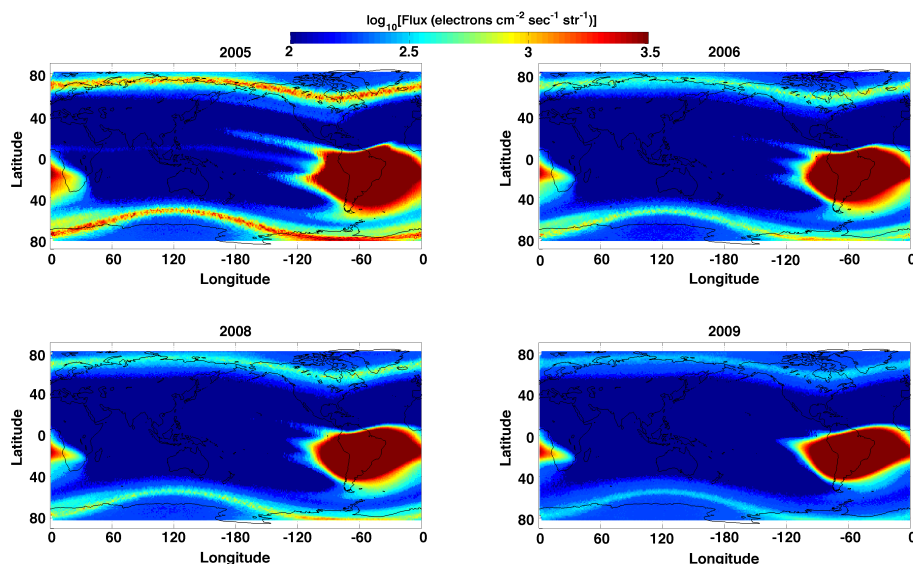


Fig. 1. World maps showing medians of >30 keV precipitating electrons observed by the 0° directed MEPED telescopes onboard POES in 2005, 2006, 2008 and 2009.

sampled simultaneously. For a detailed description of the SEM-2 instruments, see Evans and Greer (2004).

We utilise data from the MEPED 0° electron telescope (field-of-view is outward along the local zenith, parallel to the Earth-center-to-satellite radial vector). The electron telescopes are observing fluxes located inside the bounce loss cone, and thus electrons which are being lost locally toward the spacecraft direction (Rodger et al., 2010a; Rodger et al., 2010b). At this point NOAA is undertaking major new data re-processing, which will produce new data sets with derived uncertainty values. Until these have been produced we suggest a reasonable value for the measurement uncertainties is 20%, following Tan et al. (2007).

4 Results

Figure 1 shows the distribution of >30 keV electrons precipitating into the atmosphere observed by the 0° directed MEPED telescopes in 2005, 2006, 2008 and 2009. Because the year 2007 is very similar to 2008, considering electron precipitation and OH, we omitted it from the Fig. 1 (and also from Fig. 2 later) for clarity reasons. However, our analysis is conducted for the whole period between 2005–2009. These maps were produced from the 2 s resolution electron telescope data, which were corrected for proton contamination (Yando et al., 2011) using the algorithm described in Appendix A of Lam et al. (2010). For each day of the year selected, a 1° spatial resolution map of the median >30 keV fluxes was produced for each POES spacecraft in subsatellite coordinates. The median of each of these daily maps produces the median world maps shown in Fig. 1. While the Lam et al. (2010) method can generally correct for proton contam-

ination, this is not possible when the electron observations are dominated by proton counts, as expected during SPEs or in the SAMA region. The data inside the SAMA region, i.e. around 30° E– 90° W and 0° – 45° S, appears to contain an increased particle background due to a local minimum of the geomagnetic field. This however, is more likely due to contamination of the particle detectors than electron precipitation (we will discuss this in the next paragraph). In Fig. 1 the electron precipitation is confined to the geomagnetic latitudinal bands 55 – 72° N and 55 – 72° S and can occur at all geographic longitudes. However, in the SH the observed electron fluxes are consistently higher poleward of the SAMA region, i.e. the Antarctic Peninsula (AP) hotspot, which ranges in longitudinal extent from 180° W– 60° E. There is less electron precipitation at longitudes between 90° E– 180° E. The maximum difference in longitudinal EEP distribution within the range of the radiation belt in the SH is of about 150%. In the Northern Hemisphere (NH) precipitation is more homogenous through the whole longitude range with higher electron fluxes observed between 150° W– 30° W, i.e. North America (NA) hotspot. The maximum difference in longitudinal EEP distribution within the range of the radiation belt in the NH is of about 70%. A similar geographic distribution of the precipitating electrons is observed for all considered years, with a decreasing trend of electron fluxes in the radiation belts from 2005 to 2009, related to the decline in solar activity. As noted above, Fig. 1 shows a clear pattern with a local hotspot in precipitating fluxes in the AP region. This is expected, due to the changing strength of the geomagnetic field. In the AP region the magnetic field is weaker, such that the angular width of the bounce loss cone increases and electrons which were mirroring just above the atmosphere at

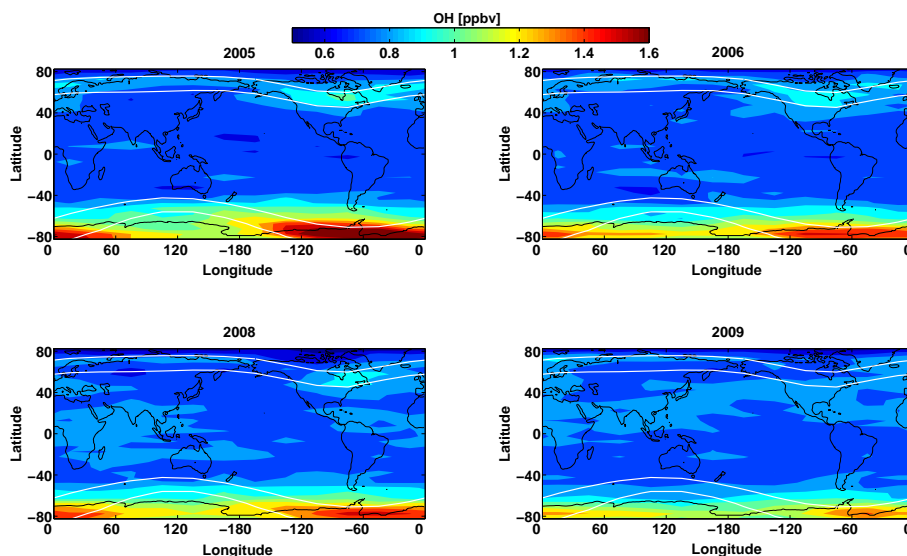


Fig. 2. World maps showing medians of nighttime OH in 2005, 2006, 2008 and 2009 averaged between 70 and 78 km. Median values were calculated for each 5° (latitude) \times 30° (longitude) bins between latitudes 82° N to 82° S and longitudes 180° W to 180° E. Approximate geomagnetic latitudes $55\text{--}72^\circ$ N/S are indicated by superimposed white lines.

other longitudes will be lost inside the atmosphere in this longitude region. The hotspot is produced by the latitude range of the radiation belts, and by the increased bounce loss cone width caused by the local minima in magnetic field strength.

To contrast Fig. 1 and hence produce a typical representation of the longitudinal OH variations caused by electron precipitation, we calculated yearly medians from nighttime OH averaged daily between 70 and 78 km. The results for 2005, 2006, 2008 and 2009 are presented in Fig. 2. At high latitudes, OH medians are 20–50 % and 30–60 % higher in the NH and SH, respectively, than those at other geographic locations. The geographic distribution of the OH high values in the NH is very similar to the distribution of precipitating electrons, i.e. OH follows geomagnetic rather than geographic latitudes. The highest OH values in the NH are confined to the longitudes from 180° W– 30° E (NAM hotspot). In the SH, there are strong local maxima at longitudes between 180° W– 30° E (AP hotspot) which partially correlate to geomagnetic latitudes $55\text{--}72^\circ$ and could be connected to the radiation belt electrons. However, OH yearly median data do not show similar enhancements at other longitudes of the radiation belt range. We investigate this matter further in Sect. 5. In order to estimate the significance of the observed maxima in the NH and SH we used the bootstrap method. For each hemisphere, we selected two 5° (latitude) \times 30° (longitude) bins inside the radiation belt region (geomagnetic latitude $55\text{--}60^\circ$ N/S) – one with low OH medians ($90\text{--}120^\circ$ E) and one with high OH medians ($60\text{--}90^\circ$ W). For each bin we calculated the median values 200 times for a random distribution of all available data points. Then the standard deviation (SD) and 95 % confidence intervals (CI) were calculated. As an example, for the year 2005 calculated median values

are robust with $SD < 3\%$ in both hemispheres. CI are: [0.94; 1.10] in the NH and [1.65; 1.81] in the SH for high OH medians bins and [0.67; 0.75] in the NH and [0.83; 0.95] in the SH for low OH medians bins. Because the 95 % confidence intervals error bars between low and high OH bins do not overlap, the difference between the two estimated medians is statistically significant with p value less than 0.05.

The OH decrease between 2005–2009 (Fig. 2) clearly shows that the changes in OH are consistent with declining solar and geomagnetic activity. Note that in the SAMA region, where MEPED-measured electron fluxes are especially high, we observe no enhancements of OH at any time, not even during the high solar activity period (e.g. 2005). This indicates that in this region there is no significant > 100 keV electron precipitation, even though precipitating fluxes generally appear to peak in this region. This is consistent with our suggestion that the signal above South America is due to the POES data contamination by protons, and in reality little precipitation is taking place, consistent with the very low geomagnetic latitudes relative to the locations of the inner and outer radiation belts. At the geomagnetic latitudes affected by electron precipitation, the mesospheric OH shows clear hemispheric asymmetry. The OH abundance in the SH is roughly twice that of the NH values for all the years considered. The reason for this behaviour is mainly due to differences in local solar time (LST) of the Aura satellite observations at the radiation belt latitudes. MLS measurements in the NH occur on average between 02:15–03:30 LST, whereas in the SH the measurements occur around midnight, i.e. between 23:30–01:15 LST. A major part of the OH production is due to daytime water vapour photodissociation, which is absent between sunset and sunrise. This leads to a decrease

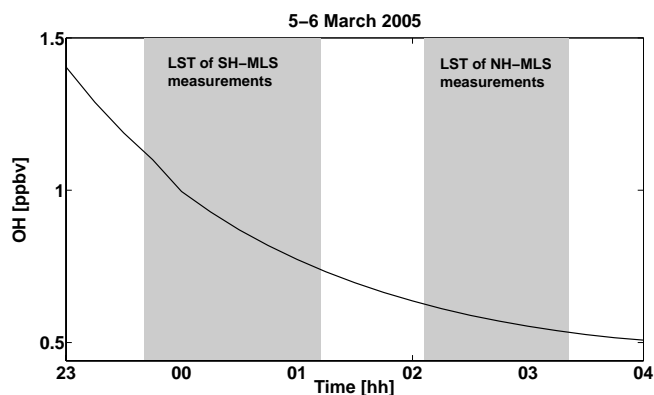


Fig. 3. OH mixing ratio from SIC model simulations for 5–6 March, 2005 at 60° N and 0° E and averaged between 70 and 78 km. Approximate LST times of MLS measurements for NH and SH are indicated by grey areas.

of OH values during nighttime. Thus, considering the difference in local time, MLS nighttime OH observations made in SH should show higher values compared to those from NH.

In order to quantitatively assess the role of LST in hemispheric discrepancies, we used the Sodankylä Ion and Neutral Chemistry model (SIC). SIC is a 1-D model of the middle atmosphere and includes a standard set of HO_x chemistry. A detailed description of the model is available in the literature (Verronen et al., 2005; Verronen, 2006; Turunen et al., 2009). A model run was made for 5–6 March 2005 at 60° N and 0° E, using MLS/Aura monthly mean values of H₂O and temperature. This setup (single location instead of contrasting NH and SH) allows us to focus on the LST effect in general without interference from, e.g. seasonal variability. Note that no electron forcing was applied to the model in order to get the general behaviour of the OH during nighttime. Figure 3 gives an example of the OH mixing ratios from a SIC model run averaged between 70 and 78 km. The modelled OH mixing ratios at LST of the satellite passage (grey areas) are of about 30–40 % higher in the SH than those in the NH. The model results suggest that LST plays a significant part in the yearly median OH hemispheric asymmetry (Fig. 2). Note that, in addition to the LST, different atmospheric in situ conditions, e.g. the amount of H₂O and temperature can also contribute to the hemispheric differences on shorter timescales. Also, solar zenith angle (SZA) differences, on average 5–10° between NH–NAM and SH–AP hotspots, could account for about 10–15 % of OH differences (see Minschwaner et al., 2011).

In order to analyse the EEP-induced longitudinal OH variations in detail, we calculated spatial distributions of nighttime OH medians between 70 and 78 km and 2005–2009 for two selected data sets, different in the strength of EEP forcing. The data sets were: (1) high energetic electron precipitation (HEEP) set, i.e. daily mean electron count rates (ECR) measured by MEPED > 100 counts/s, 51 days of

data in total; (2) low energetic electron precipitation (LEEP) set, ECR < 5 counts s⁻¹, 1340 days in total. Contrasting these two data sets allows us to see what proportion of the longitudinal OH-hotspots is caused by EEP. The results are presented in Fig. 4. We do not show the ECR maps for selected cases as they show the same longitudinal structure as maps presented in Fig. 1, with more homogeneously distributed fluxes in the NH for the HEEP case. During the LEEP period, high OH values are centered around the geographic pole with maximum OH inside the radiation belt in the AP sector (bottom right panel), while in the NH there is slightly more OH over the NAM sector compared to other longitudes (top right panel). The enhanced values in the SH in the Antarctic Peninsula (AP) sector could be connected to the steady drizzle of radiation belt electrons continuously affecting the mesosphere even during LEEP conditions (Clilverd et al., 2010b), as well as different atmospheric conditions (discussed in the next paragraph). During the HEEP periods, SH–OH longitudinal structure is preserved, i.e. OH clearly peaks in the AP sector. Note that OH enhancements are also observed at other longitudes in the radiation belt region, i.e. 75–165° E, but the amplitudes of these enhancements are lower than in the AP sector. This cannot be seen from yearly medians presented in Fig. 2. In the NH, OH enhancements due to EEP are more equally distributed between 90° W–90° E, i.e. NAM and North Asia (NAs) sectors, similar to the observed ECR. In order to estimate the significance of the observed HEEP enhancements in the NH and SH we used the bootstrap method in the same way as in the case of yearly OH medians (see description of Fig. 2). In this case, we have selected 5° (latitude) × 30° (longitude) bins inside the radiation belt region (geomagnetic latitude 55–60° N/S and 60–90° W) and outside the radiation belt region (40–45° N/S and 0–30° E). Inside the radiation belts bins, SD < 12 % and CI = [1.05–1.42] in the NH and SD < 8 % and CI = [1.80; 2.24] in the SH. Outside the radiation belts' latitudes, SD values are the same and CI = [0.68–0.97] in the NH and SD < 8 % and CI = [0.62; 0.99] in the SH. Again, the 95 % confidence intervals for bins inside and outside the radiation belt latitudes do not overlap, which suggest that the difference between the two estimated medians is statistically significant with *p* value less than 0.05.

As it was mentioned in the previous paragraph, the enhanced values in the SH (see Fig. 4) could be connected to the steady drizzle of radiation belt electrons but also the differences in H₂O and temperature could cause some of the observed OH longitudinal variability. Therefore, we examine their possible role in the observed OH enhancements in the AP sector. Figure 5 shows H₂O (left panel) and temperature (right panel) medians calculated for the LEEP data set, i.e. daily mean ECR < 5 counts s⁻¹. Before calculating the median values, nighttime mean H₂O and temperature measurements were averaged between 70 and 76 km. In the SH, low H₂O and high temperature values are centered around the geographic pole. In the radiation belt latitudes, low H₂O

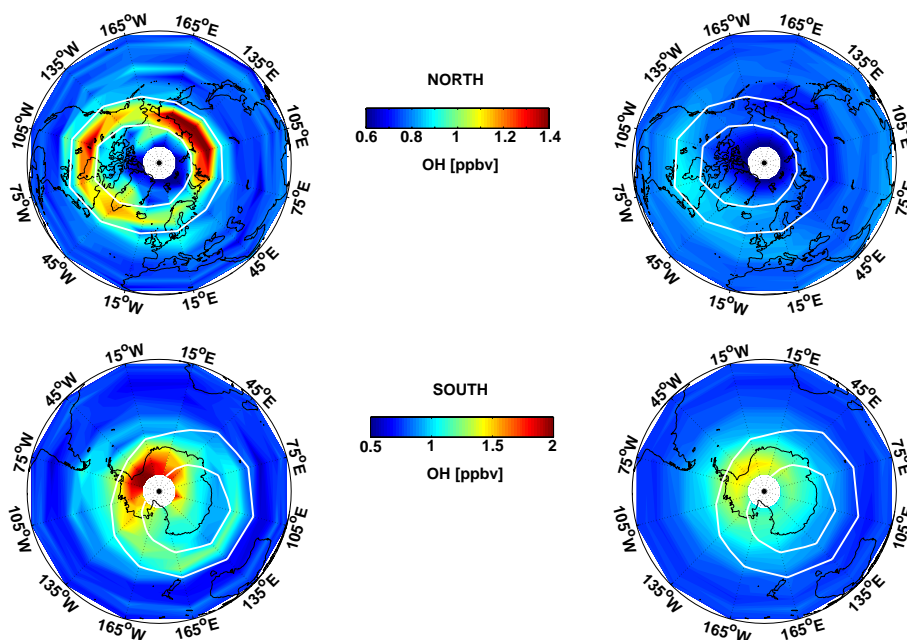


Fig. 4. Top panels: spatial distribution of OH medians in the NH calculated for the days with: (1) ECR > 100 counts/s (left panel) and (2) ECR < 5 counts/s (right panel) for the time period January 2005–December 2009 and altitude range 70–78 km. Bottom panels as top panels for the SH. Median values were calculated for each 5 (latitude) \times 30 (longitude) degree bin between latitudes 82° N to 82° S and longitudes 180° W to 180° E. Approximate geomagnetic latitudes 55–72° N/S are indicated by superimposed white lines.

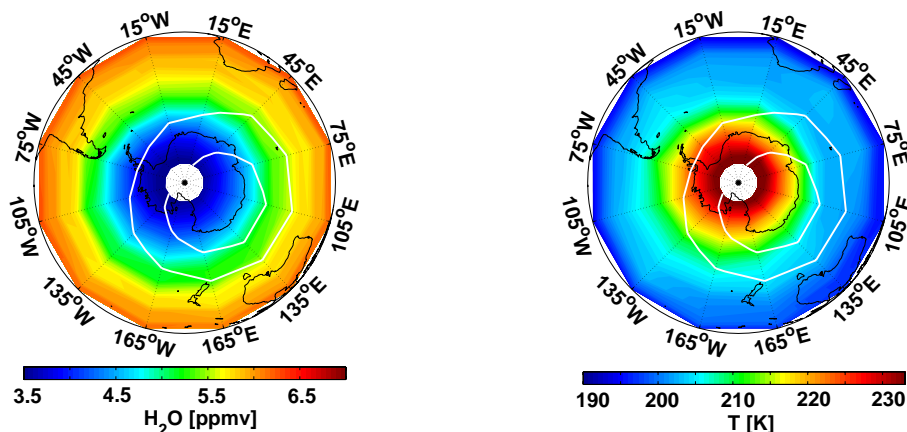


Fig. 5. Spatial distribution of nighttime H₂O (left panel) and temperature (right panel) medians during low EEP period (case II) averaged between 70 and 76 km. Median values were calculated for each 5 (latitude) \times 30 (longitude) degree bins between latitudes 82° N to 82° S and longitudes 180° W to 180° E. Approximate geomagnetic latitudes 55–72° N/S are indicated by superimposed white lines.

corresponds to the high OH values (see bottom right panel of the Fig. 4) and therefore the H₂O can not explain the OH enhancement in the AP region. Because temperature and OH are positively correlated at altitudes below 80 km (Damiani et al., 2010a), OH enhancement in the AP sector can be partially explained by the higher temperature observed in this region. In order to quantify the sensitivity of OH to the temperature during LEEP and separate them from EEP-induced OH enhancements, we again used the SIC model. All model runs were made between 5 (12:00 UT)–6 (12:00 UT) March

2005 at 60° N/65° S and 0° E with high electron-precipitation produced ionization rates, i.e. 1000 cm⁻³ s⁻¹. First, we made model runs using MLS monthly mean values of the temperature, i.e. 100 % T . Then we changed the temperature according to the longitudinal variability observed during LEEP, i.e. 110 % T (see Fig. 5). The obtained results (not shown here) indicate that increasing temperature by 10 % (similar to that seen in the region around the AP region) increases nighttime OH mixing ratio on average by about 15–25%. In addition, the average difference between longitudinal distribution of

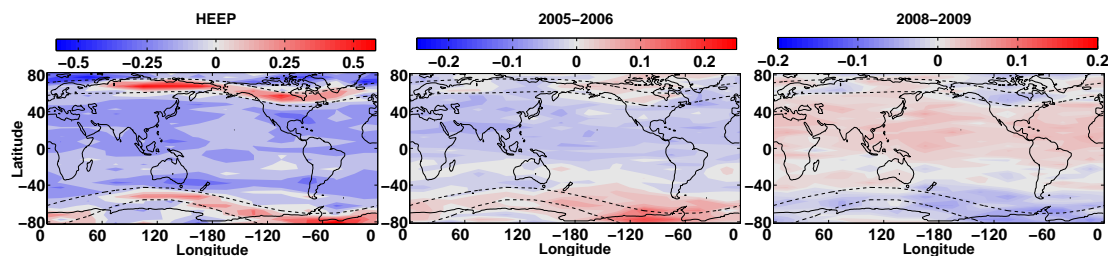


Fig. 6. OH anomalies for 3 selected data sets: (1) HEEP (left panel), (2) ECR < 5 between 2005–2006 (middle panel) and (3) ECR < 5 between 2008–2009 (right panel).

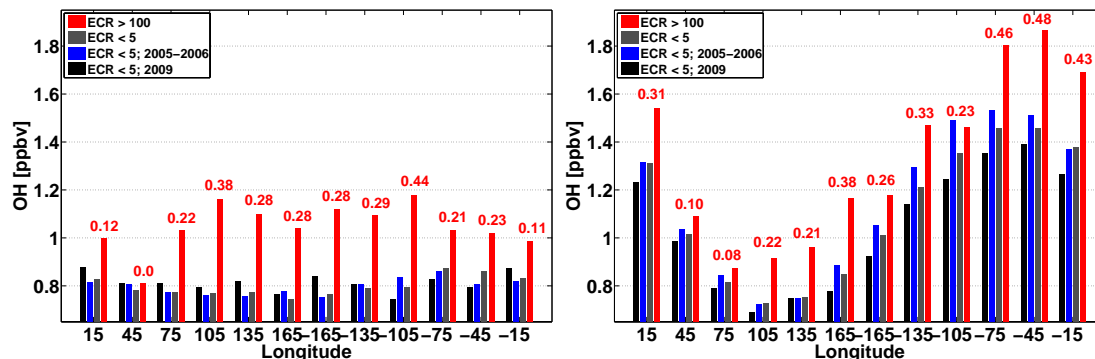


Fig. 7. Longitudinal variations of OH medians at geomagnetic latitudes $55\text{--}72^\circ\text{N}$ (left panel) and $55\text{--}72^\circ\text{S}$ (right panel) and altitudes between 70 and 78 km for 4 selected cases (see description in the text). Numbers indicate the absolute (ppbv, red) difference between OH during high EEP (case I) and the OH during the low geomagnetic activity (case IV).

SZA of about 20° , can account for about 25–30 % of longitudinal variability. Therefore, the stronger OH response in the AP sector (80 % higher than at the other longitudes) can be partly explained by different atmospheric conditions, but it is also likely connected to the peak in electron precipitation forcing occurring in the same spatial region. Note that LST of MLS observations is dependent on geographic latitude, which causes a LST difference of about 2.5 h between AP (75°W) and 120°E . Based on SIC model test calculations, the measured OH concentrations in the AP region are expected to be in general lower than at 120°E because of the LST difference, which would partly cancel out the estimated OH effect of atmospheric background variability (40–55%). However, because the OH effects of atmospheric background variability (including those due to SZA, LST, T , and H_2O) are not easily separated and because our model runs are made for a few typical cases only we retain our estimation of atmospheric background influence as an upper limit value.

In Fig. 6 we plot OH anomalies for 3 selected data sets: (1) HEEP (left panel), (2) ECR < 5 between 2005–2006 (middle panel) and (3) ECR < 5 between 2008–2009 (right panel). For each data set the OH background was subtracted, i.e. the mean of days with ECR < 5 (2005–2009). The figure shows that during HEEP, OH enhancements follow radiation belt latitudes. In the NH, the OH distribution is more homogeneous, while in the SH the AP sector shows larger OH anomalies

compared to other longitudes. The OH anomalies in the AP region during the declining phase of the solar activity (2005–2006) suggest a possible influence from study drizzle of electrons. Between 2008–2009, i.e. during prolonged solar minimum (lower geomagnetic activity), no OH enhancement is observed in the AP region. The significance of the OH enhancements in the AP region in the SH for case 1 and 2 was tested using the bootstrap method. Obtained SD and CI are: 20%/[0.4; 0.8] and 30%/[0.1; 0.3] for 1 and 2, respectively.

Summarising our analysis, Fig. 7 shows the radiation belt OH medians for 4 data sets: (i) days (30 for NH, 40 for SH) between 2005–2009 with ECR > 100 counts s^{-1} (high precipitation, again termed HEEP), (ii) days (723 for NH, 767 for SH) between 2005–2009 with ECR < 5 counts s^{-1} (low precipitation, termed LEEP), (iii) days (264 for NH, 267 for SH) between 2005–2006 with ECR < 5 counts s^{-1} , (low precipitation, high geomagnetic activity years), (iv) days (141 for NH, 163 for SH) in 2009 with ECR < 5 counts/s (low precipitation, low geomagnetic activity years). Note that only days with full longitudinal coverage were taken into account, which basically excludes the summertime periods. In addition to the HEEP (I) and LEEP (II) which we already considered when discussing Fig. 4, cases III and IV are needed to investigate possible influences from the steady drizzle of radiation belt electrons continuously affecting the mesosphere even during LEEP conditions. For all considered

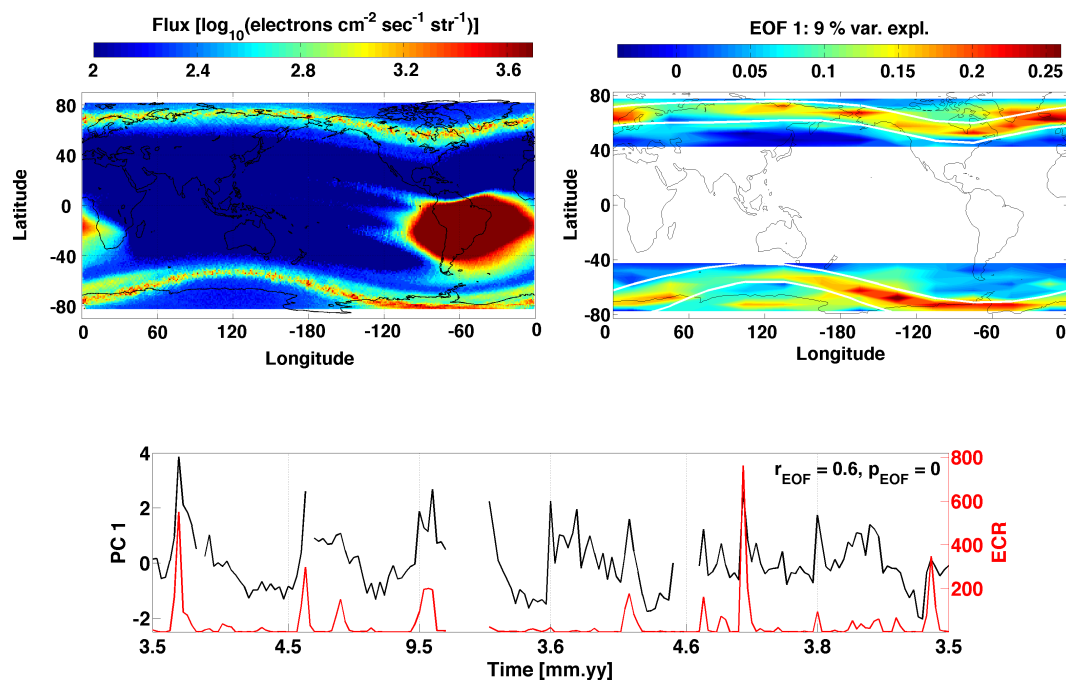


Fig. 8. Top left panel: World maps showing medians of > 30 keV precipitating electrons observed by the 0° directed MEPED telescopes onboard POES for 6 selected months (see description in the text). Top right panel: first EOF mode as a function of latitude and longitude for selected months between January 2005–December 2009. Numbers in percent indicate variance represented by each mode to the total variance. Bottom panel: the PC (black lines) of the first EOF mode. Red line represents the daily mean electron count rates. Approximate geomagnetic latitudes 55–72° N/S are indicated by superimposed white lines.

cases (I–IV), SH–OH shows stronger longitudinal variability, which is primarily caused by geomagnetic latitude selection, and therefore, different atmospheric conditions (H₂O, temperature and SZA). The absolute/relative OH differences between case I and IV are of about the same magnitude in the NH and SH, varying from 0.04–0.46 ppbv/0–60%. The maximum OH enhancements in the NH are more equally distributed, i.e. confined to the longitudinal range between 90° E–90° W. In the SH, the largest increase is seen in the AP sector, i.e. 180° W–0° E which is likely to be connected to the stronger EEP forcing in this region. In order to estimate the significance of the OH enhancements for the ECR > 100 case, we again used the bootstrap method and calculated SD and CI for each of the longitudes presented in Fig. 7. In the NH, SD varies between 7–12% with CI between [0.7–1; 1.0–1.35] for all longitudes. In the SH, SD varies between 3–8% with CI=[0.8–1.0; 1.0–1.3] for longitudes 45° E–165° W and CI=[1.4–1.6; 1.7–2.2] for longitudes 135° W–15° E. For all longitudes except 45° E in the NH and 45–75° E in the SH, the 95% confidence interval error bars calculated for ECR > 100 do not overlap with those for ECR < 5, and the estimated medians are statistically different with p value less than 0.05. Comparison between case III and IV shows that in the SH, in the AP region, OH values are about 5–20% higher during the periods selected by case III. This again may indicate steady drizzle of radiation belt electrons around the AP

in the SH. In the NH, OH mean values during the periods selected by cases III and IV are comparable.

Finally, to further support our conclusions, we analysed the OH data again using Empirical Orthogonal Function method. The EOF method decomposes the data set into a set of orthogonal basis functions in order to find the structures (EOF modes) that explain the maximum amount of variance in a two dimensional data set as well as their time variations, i.e. principal components (PC). More details about can be found in van Storch and Zwiers (1999, and references therein). The EOF analysis was conducted for 6 selected months between 2005–2009, i.e. March–April 2005, September 2005, March–April 2006 and March 2008. The months were selected for 2 reasons: (1) high EEP events were observed for each month; and (2) full global coverage during spring/autumn periods in both hemispheres with similar numbers of profiles selected and similar in situ atmospheric conditions. The nighttime OH data were divided into 5 (latitude) × 30 (longitude) degree bins. The OH monthly mean was removed, leaving anomalies that retain variation on daily to interannual timescales. The leading EOF spatial pattern and EOF time series were calculated for the anomaly fields averaged between 70 and 78 km. Both, EOF and PC were normalised and the physical units follow normal convention of presenting EOFs. The results of EOF analysis, i.e. first EOF along with the variance explained (%) and

corresponding PC 1, are shown in Fig. 8. Figure 8 also shows the median distribution of > 30 keV electrons precipitating into the atmosphere observed by the 0° directed MEPED for the same months EOF analysis was conducted. Note that the OH measurements from the equatorial regions, i.e. 45°S – 45°N were excluded from analysis in order to avoid possible impact from other factors (for example tides) that could affect the OH variation.

The observed electron precipitation seen in the upper left-hand panel of this figure is similar to the yearly medians presented in Fig. 1 except that it has a more pronounced longitudinal structure. EEP is clearly higher in the AP region and slightly higher between 150°E – 0°W in the NH in the magnetic latitudinal band 55 – 72°N/S . The first EOF (right top panel of Fig. 8) also has pronounced structures at geomagnetic latitudes connected to the radiation belts (55 – 72°N/S) and appears to be associated with the spatial variations in electron precipitation. The spatial patterns of the OH changes do not extend to other latitudes and follow the radiation belt areas much more closely than the yearly median presented in Fig. 2. EOF 1 constitutes 9% of the total variance, and this mode clearly dominates the OH variation after a strong global seasonal component was removed. The principal component (PC 1) related to the first EOF follows the ECR variability (bottom panel of Fig. 8). The correlation between amplitude of the PC 1 and ECR is $r_{\text{EOF}} = 0.6$. The statistical robustness of the correlation was determined by calculating the p value (t test). The resulting $p < 0.01$, i.e. the random chance probability of getting such correlation for the data sets when the true correlation is zero is less than 1%. Note that the enhanced PC 1 values at the beginning of March 2006 are connected to the enhanced OH values at latitudes $> 70^\circ\text{N}$ and longitudes 0 – 120°W , i.e. outside radiation belt latitudes. Similar OH enhancement, again outside the radiation belt latitudes, is observed in March 2008 at latitudes $> 70^\circ\text{S}$ and longitudes 90°E – 120°W . In the SH, the reason for such OH enhancement is unclear. In the NH, it could be connected to the descent of OH maximum layer, which occurred in 2006 after a sudden stratospheric warming event (Damiani et al., 2010a).

These results indicate that first EOF is associated with EEP. EOF 1 not only reflects an enhancement of OH at latitudes affected by EEP but also captures its longitudinal variations, i.e. maximum increases confined to the longitudinal band 150°E – 30°W in the NH and 180°W – 60°E in the SH (see Fig. 4). We analysed also the second and third EOF patterns (not shown). However, these sum up to less than 4% of the total variance and the patterns do not correlate with EEP. They are more likely connected to the noise.

5 Conclusions

Using measurements from the MLS/Aura and MEPED/POES between 2005–2009, we have studied longitudinal variations of nighttime OH and their link to energetic electron precipitation. The time period analysed here coincided with a declining phase of solar activity and an extended solar minimum, and thus consists mainly of HSSWS-driven storms. Our analysis shows, that at geomagnetic latitudes 55 – 72°N/S and altitudes between 70 and 78 km, there are spatial hotspots in the mesospheric OH variations due to energetic electron precipitation.

In the SH, an OH hotspot is located in the AP region, i.e. in a longitudinal band between 150°W – 60°E . At those longitudes, EEP observed by POES, as well as the OH enhancement are the highest. Because the atmospheric in situ conditions can explain only part of the total 80% of OH longitudinal variations (15–25% H_2O and temperature, 25–30% SZA), the OH hotspot in this sector is likely to be connected to stronger electron forcing. Also, increased OH values in this region during the period of low EEP but higher geomagnetic activity suggest the effect of a steady drizzle of radiation belt electrons during the quiet time conditions. EOF analysis has shown similar pronounced structures at geomagnetic latitudes connected to the radiation belts (55 – 72°S). The first EOF mode constitutes 9% of the total variance, and clearly reflects an enhancement of OH at latitudes affected by EEP as well as its longitudinal variations, i.e. a maximum amplitude confined to the longitudinal band 150°W – 60°E . Note that even though MEPED measures very high electron count rates inside SAMA, this does not seem to correspond to any significant precipitation, i.e. no OH enhancement is observed in that region.

In the NH, EEP is more homogenous over the whole longitude range with slightly higher electron fluxes observed between 180°W – 0°E , i.e. over the NAM sector. The distribution of OH yearly medians is roughly confined to the same longitudinal band 150°W – 30°E , but the OH medians during HEEP show different spatial behaviour, i.e. an OH hotspot extends from NAM to the NAs sector (90°E – 90°W). The first EOF mode clearly reflects the OH enhancement with the maximum amplitude roughly confined to the longitudinal band 150°W – 30°E .

Our analysis has shown a significant role of the particle precipitation in the OH distribution at latitudes connected to the radiation belt, which is especially important in the SH due to the local weakness in the Earth's magnetic field. Taking into account the OH longitudinal variations due to the energetic electrons precipitation is important from the point of view of the atmospheric modelling in order to better represent polar regions.

Acknowledgements. M. E. Andersson would like to thank Marko Laine for helpful comments. The work of M. E. Andersson and P. T. Verronen was supported by the Academy of Finland through the projects #136225, #140888, and #272782 (SPOC: Significance of Energetic Electron Precipitation to Odd Hydrogen, Ozone, and Climate). The work of C. J. Rodger was supported by the New Zealand Marsden fund. The work of S. Wang was supported by the NASA Aura Science Team program.

Edited by: G. Stiller

References

- Andersson, M. E., Verronen, P. T., Wang, S., Rodger, C. J., Clilverd, M. A., and Carson, B.: Precipitating radiation belt electrons and enhancements of mesospheric hydroxyl during 2004–2009, *J. Geophys. Res.*, 117, D09304, doi:10.1029/2011JD017246, 2012.
- Borovsky, J. E. and Denton, M., H.: Differences between CME-driven storms and CIR-driven storms, *J. Geophys. Res.*, 111, A07S08, doi:10.1029/2005JA011447, 2006.
- Clilverd, M. A., Rodger, C. J., Moffat-Griffin, T., Spanswick, E., Breen, P., Menk, F. W., Grew, R. S., Hayashi, K., and Mann, I. R.: Energetic outer radiation belt electron precipitation during recurrent solar activity, *J. Geophys. Res.*, 115, A08323, doi:10.1029/2009JA015204, 2010.
- Clilverd, M. A., Rodger, C. J., Gamble, R. J., Ulich, Th., Raita, T., Seppälä, A., Green, J. C., Thomson, N. R., Sauvaud, J.-A., and Parrot, M.: Ground-based estimates of outer radiation belt energetic electron precipitation fluxes into the atmosphere, *J. Geophys. Res.*, 115, A12304, doi:10.1029/2010JA015638, 2010b.
- Damiani, A., Storini, M., Laurenza, M., and Rafanelli, C.: Solar particle effects on minor components of the Polar atmosphere, *Ann. Geophys.*, 26, 361–370, doi:10.5194/angeo-26-361-2008, 2008.
- Damiani, A., Storini, M., Santee, M. L., and Wang, S.: Variability of the nighttime OH layer and mesospheric ozone at high latitudes during northern winter: influence of meteorology, *Atmos. Chem. Phys.*, 10, 14583–14610, doi:10.5194/acpd-10-14583-2010, 2010a.
- Damiani, A., Storini, M., Santee, M. L., and Wang, S.: The hydroxyl radical as an indicator of SEP fluxes in the high-latitude terrestrial atmosphere, *Adv. Space Res.*, 46, 1225–1235, doi:10.1016/j.asr.2010.06.022, 2010b.
- Evans, D. S. and Greer, M. S.: Polar Orbiting environmental satellite space environment monitor – 2 instrument descriptions and archive data documentation, NOAA Technical Memorandum version 1.4, Space Environment Laboratory, Colorado, 2004.
- Funke, B., Baumgaertner, A., Calisto, M., Egorova, T., Jackman, C. H., Kieser, J., Krivolutsky, A., López-Puertas, M., Marsh, D. R., Reddmann, T., Rozanov, E., Salmi, S.-M., Sinnhuber, M., Stiller, G. P., Verronen, P. T., Versick, S., von Clarmann, T., Vyushkova, T. Y., Wieters, N., and Wissing, J. M.: Composition changes after the “Halloween” solar proton event: the High-Energy Particle Precipitation in the Atmosphere (HEPPA) model versus MIPAS data intercomparison study, *Atmos. Chem. Phys.*, 11, 9089–9139, doi:10.5194/acp-11-9089-2011, 2011.
- Heaps, M. G.: The effect of a solar proton event on the minor neutral constituents of the summer polar mesosphere, *Tech. Rep.* ASL-TR0012, US Army Atmos. Sci. Lab., White Sands Missile Range, N. M., 1978.
- Jackman, C. H., Marsh, D. R., Vitt, F. M., Roble, R. G., Randall, C. E., Bernath, P. F., Funke, B., López-Puertas, M., Versick, S., Stiller, G. P., Tylka, A. J., and Fleming, E. L.: Northern Hemisphere atmospheric influence of the solar proton events and ground level enhancement in January 2005, *Atmos. Chem. Phys.*, 11, 6153–6166, doi:10.5194/acp-11-6153-2011, 2011.
- Lam, M. M., Horne, R. B., Meredith, N. P., Glauert, S. A., Moffat-Griffin, T., and Green, J. C.: Origin of energetic electron precipitation > 30 keV into the atmosphere, *J. Geophys. Res.*, 115, A00F08, doi:10.1029/2009JA014619, 2010.
- Lambert, A., Read, W. G., Livesey, N. J., Santee, M. L., Manney, G. L., Froidevaux, L., Wu, D. L., Schwartz, M. J., Pumphrey, H. C., Jimenez, C., Nedoluha, G. E., Cofield, R. E., Cuddy, D. T., Daffer, W. H., Drouin, B. J., Fuller, R. A., Jarnot, R. F., Knosp, B. W., Pickett, H. M., Perun, V. S., Snyder, W. V., Stek, P. C., Thurstans, R. P., Wagner, P. A., Waters, J. W., Jucks, K. W., Toon, G. C., Stachnik, R. A., Bernath, P. F., Boone, C. D., Walker, K. A., Urban, J., Murtagh, D., Elkins, J. W., and Atlas, E.: Validation of the Aura Microwave Limb Sounder middle atmosphere water vapor and nitrous oxide measurements, *J. Geophys. Res.*, 112, D24S32, doi:10.1029/2007JD008724, 2007.
- Livesey, N. J., Read, W. G., Froidevaux, L., Lambert, A., Manney, G. L., Pumphrey, H. C., Santee, M. L., Schwartz, M. J., Wang, S., Cofield, R. E., Cuddy, D. T., Fuller, R. A., Jarnot, R. F., Jiang, J. H., Knosp, B. W., Stek, P. C., Wagner, P. A., and Wu, D. L.: EOS MLS Version 3.3 Level 2 data quality and description document, JPL D-33509, Jet Propulsion Laboratory, Version 3.3x-1.0, 18 January, 2011.
- Minschwaner, K., Manney, G. L., Wang, S. H., and Harwood, R. S.: Hydroxyl in the stratosphere and mesosphere – Part 1: Diurnal variability, *Atmos. Chem. Phys.*, 11, 955–962, doi:10.5194/acp-11-955-2011, 2011.
- Pickett, H. M., Drouin, B. J., Canty, T., Salawitch, R. J., Fuller, R. A., Perun, V. S., Livesey, N. J., Waters, J. W., Stachnik, R. A., Sander, S. P., Traub, W. A., Jucks, K. W., and Minschwaner, K.: Validation of Aura Microwave Limb Sounder OH and HO₂ measurements, *J. Geophys. Res.*, 113, D16S30, doi:10.1029/2007JD008775, 2008.
- Reeves, G. D., McAdams, K. L., Friedel, R. H. W., and O’Brien, T. P.: Acceleration and loss of relativistic electrons during geomagnetic storms, *Geophys. Res. Lett.*, 30, 1529, doi:10.1029/2002GL016513, 2003.
- Richardson, I. G., Cliver, E. W., and Cane, H. V.: Sources of geomagnetic activity over the solar cycle: Relative importance of coronal mass ejections, high-speed streams, and slow solar wind, *J. Geophys. Res.*, 105, 18203–18213, 2000.
- Richardson, I. G., Cliver, E. W., and Cane, H. V.: Sources of geomagnetic storms for solar minimum and maximum conditions during 1972–2000, *Geophys. Res. Lett.*, 28, 13, 2569–2572, 2001.
- Rodger, C. J., Clilverd, M. A., Green, J. C., and Lam, M. M.: Use of POES SEM-2 observations to examine radiation belt dynamics and energetic electron precipitation into the atmosphere, *J. Geophys. Res.*, 115, A04202, doi:10.1029/2008JA014023, 2010a.
- Rodger, C. J., Carson, B. R., Cummer, S. A., Gamble, R. J., Clilverd, M. A., Sauvaud, J.-A., Parrot, M., Green, J. C., and Berthelier, J.-J.: Contrasting the efficiency of radiation belt

- losses caused by ducted and non-ducted whistler mode waves from ground-based transmitters, *J. Geophys. Res.*, 115, A12208, doi:10.1029/2010JA015880, 2010b.
- Schwartz, M. J., Lambert, A., Manney, G. L., Read, W. G., Livesey, N. J., Froidevaux, L., Ao, C. O., Bernath, P. F., Boone, C. D., Cofield, R. E., Daffer, W. H., Drouin, B. J., Fetzer, E. J., Fuller, R. A., Jarnot, R. F., Jiang, J. H., Jiang, Y. B., Knosp, B. W., Krüger, K., Li, J.-L. F., Mlynczak, M. G., Pawson, S., Russell III, J. M., Santee, M. L., Snyder, W. V., Stek, P. C., Thurstans, R. P., Tompkins, A. M., Wagner, P. A., A., W. K., Waters, J. W., and Wu, D. L.: Validation of the Aura Microwave Limb Sounder temperature and geopotential height measurements, *J. Geophys. Res.*, 113, D15S11, doi:10.1029/2007JD008783, 2008.
- Sinnhuber, M., Nieder, H., and Wieters, N.: Energetic particle precipitation and the chemistry of the mesosphere/lower thermosphere, *Surv. Geophys.*, 33, 1281–1334, doi:10.1007/s10712-012-9201-3, 2012.
- Solomon, S., Rusch, D. W., Gérard, J.-C., Reid, G. C., and Crutzen, P. J.: The effect of particle precipitation events on the neutral and ion chemistry of the middle atmosphere: II. Odd hydrogen, *Planet. Space Sci.*, 8, 885–893, 1981.
- Tan, L. C., Fung, S. F., and Shao, X.: NOAA/POES MEPED Data Documentation: NOAA-5 to NOAA-14 Data Reprocessed at GSFC/SPDF, NASA, Space Physics Data Facility, 2007.
- Thorne, R. M.: Energetic radiation belt electron precipitation - A natural depletion mechanism for stratospheric ozone, *Science*, 195, 287–289, 1977.
- Turunen, E., Verronen, P. T., Seppälä, A., Rodger, C. J., Clilverd, M. A., Tamminen, J., Enell, C.-F., and Ulich, T.: Impact of different precipitation energies on NO_x generation during geomagnetic storms, *J. Atmos. Sol.-Terr. Phys.*, 71, 1176–1189, doi:10.1016/j.jastp.2008.07.005, 2009.
- van Storch, H. and Zwiers, F. W.: *Statistical Analysis in Climate Research*, Cambridge University Press, New York, 289–316, 1999.
- Verronen, P. T.: Ionosphere-atmosphere interaction during solar proton events, no. 55 in *Finnish Meteorological Institute Contributions*, Finnish Meteorological Institute, Helsinki, Finland, ISBN:952-10-3111-5, 2006.
- Verronen, P. T. and Lehmann, R.: Analysis and parameterisation of ionic reactions affecting middle atmospheric HO_x and NO_y during solar proton events, *Ann. Geophys.*, 31, 909–956, doi:10.5194/angeo-31-909-2013, 2013.
- Verronen, P. T., Seppälä, A., Clilverd, M. A., Rodger, C. J., Kyrölä, E., Enell, C.-F., Ulich, T., and Turunen, E.: Diurnal variation of ozone depletion during the October–November 2003 solar proton events, *J. Geophys. Res.*, 110, A09S32, doi:10.1029/2004JA010932, 2005.
- Verronen, P. T., Seppälä, A., Kyrölä, E., Tamminen, J., Pickett, H. M., and Turunen, E.: Production of odd hydrogen in the mesosphere during the January 2005 solar proton event, *Geophys. Res. Lett.*, 33, L24811, doi:10.1029/2006GL028115, 2006.
- Verronen, P. T., Rodger, C. J., Clilverd, M. A., Pickett, H. M., and Turunen, E.: Latitudinal extent of the January 2005 solar proton event in the Northern Hemisphere from satellite observations of hydroxyl, *Ann. Geophys.*, 25, 2203–2215, doi:10.5194/angeo-25-2203-2007, 2007.
- Verronen, P. T., Rodger, C. J., Clilverd, M. A., and Wang, S.: First evidence of mesospheric hydroxyl response to electron precipitation from the radiation belts, *J. Geophys. Res.*, 116, D07307, doi:10.1029/2010JD014965, 2011.
- Waters, J. W., Froidevaux, L., Harwood, R. S., Jarnot, R. F., Pickett, H. M., Read, W. G., Siegel, P. H., Cofield, R. E., Filipiak, M. J., Flower, D. A., Holden, J. R., Lau, G. K., Livesey, N. J., Manney, G. L., Pumphrey, H. C., Santee, M. L., Wu, D. L., Cuddy, D. T., Lay, R. R., Loo, M. S., Perun, V. S., Schwartz, M. J., Stek, P. C., Thurstans, R. P., Boyles, M. A., Chandra, K. M., Chavez, M. C., Chen, G.-S., Chudasama, B. V., Dodge, R., Fuller, R. A., Girard, M. A., Jiang, J. H., Jiang, Y., Knosp, B. W., Labelle, R. C., Lam, J. C., Lee, A. K., Miller, D., Oswald, J. E., Patel, N. C., Pukala, D. M., Quintero, O., Scaff, D. M., Vansnyder, W., Tope, M. C., Wagner, P. A., and Walch, M. J.: The Earth Observing System Microwave Limb Sounder (EOS MLS) on the Aura satellite, *IEEE Trans. Geosci. Remote Sens.*, 44, 1075–1092, doi:10.1109/TGRS.2006.873771, 2006.
- Yando, K., Millan, R. M., Green, J. C., and Evans, D. S.: A Monte Carlo simulation of the NOAA POES Medium Energy Proton and Electron Detector instrument, *J. Geophys. Res.*, 116, A10231, doi:10.1029/2011JA016671, 2011.